Appl. Phys. A 81, 1065–1071 (2005)
DOI: 10.1007/s00339-004-2949-7

Applied Physics A
Materials Science & Processing

F. GONELLA[1,✉]
A. QUARANTA[2]
S. PADOVANI[3]
C. SADA[3]
F. D'ACAPITO[4]
C. MAURIZIO[4]
G. BATTAGLIN[1]
E. CATTARUZZA[1]

Copper diffusion in ion-exchanged soda-lime glass

[1] INFM, Dip. di Chimica Fisica, Università Ca' Foscari di Venezia, Dorsoduro 2137, 30123 Venezia, Italy
[2] INFM, Dipartimento di Ingegneria dei Materiali, Università di Trento, via Mesiano 77, 38050 Povo, Trento, Italy
[3] INFM-MATIS, Dipartimento di Fisica, Università di Padova, via Marzolo 8, 35131, Padova, Italy
[4] INFM, ESRF, GILDA-CRG, B.P. 220, 38043, Grenoble, France

Received: 15 January 2004/Accepted: 31 May 2004
Published online: 29 July 2004 •

ABSTRACT Cu-alkali ion exchange in silicate glasses gives rise to a peculiar copper distribution, with the presence of both the Cu^{2+} and Cu^{+} oxidation states. Grazing incidence X-ray absorption near-edge structure spectroscopy and secondary ion mass spectrometry were performed on different ion-exchanged samples. The results show that the Cu^{2+}/Cu^{+} ratio is strongly depth-dependent. The relative presence of the two species throughout the exchanged region turns out to be governed by their different diffusion regimes, while the chemistry of the redox process is shown to play a minor role. A phenomenological model is proposed to describe the diffusion process.

PACS 61.10.Ht; 61.43.Fs; 82.65.+r; 67.80.Mg

1 Introduction

Metal-alkali ion exchange in glass has been widely used to dope silicate glasses [1]. The process is realized by immersing silicate glass slides in a molten salt bath containing the dopant ions, which replace alkali ions of the glass matrix. Ion exchange with copper has in particular attracted new attention for the blue-green luminescence properties of copper-doped glasses [2, 3], useful for laser technology, as well as for the third-order nonlinear optical features of copper nanoclusters in glass [4–6]. The former property is due to the copper ions dispersed in the glass matrix in the Cu^{+} oxidation state [7], while the latter to the formation of Cu metallic nanoclusters. In this framework, the knowledge of the distribution of copper oxidation states inside the treated glass is a central issue for both the understanding of the incorporation process and for application purposes. At present, only a few studies have been dedicated to ion exchange with copper [8–12], and several open questions yet remain concerning the copper behavior inside the glass upon ion exchange. Because of the possible presence of different oxidation states, namely, Cu^{+}, Cu^{2+} and Cu^{0}, copper distribution within the matrix follows a rather complex behavior [11], critically depending on both glass and bath composition as well as on the process parameters. In this work, X-ray absorption fine structure (XAFS) spectroscopy in grazing incidence mode and secondary ion mass spectrometry (SIMS) were performed on soda-lime glasses after Cu-alkali ion exchange. The combined use of these analytical tools allowed us to define an exhaustive picture of the microscopic structure reached after the doping process. In particular, XAFS spectroscopy provides detailed depth-dependent information on the local structure, allowing to relate the observed copper distribution features to the local composition and structure [13]. A phenomenological model of the diffusion process was developed to account for the anomalous distribution of the copper species outlined by the experimental analysis techniques.

✉ Fax: +39-041/234-8594, E-mail: gonella@unive.it

2 Experimental

Ion exchange was realized by immersing commercial soda-lime (wt. % 69.6 SiO_2, 15.2 Na_2O, 1.1 K_2O, 6.5 CaO, 5.1 MgO, 1.8 Al_2O_3, 0.4 SO_3, 0.2 TiO_2 and 0.1 traces) glass slides in a molten salt bath of $CuSO_4$:Na_2SO_4 (54:46 mol %); the process was carried out at 545 °C for 10 minutes.

X-ray absorption spectroscopy was performed for the Cu *K*-edge (8979 eV), on the Italian beamline GILDA of the European Synchrotron Radiation Facility (ESRF), with a bending magnet device source. The sagittally focusing monochromator [14], used in the so-called dynamical focusing mode, was equipped with two Si(311) crystals. Harmonic rejection was achieved by using two Pd coated mirrors with an energy cutoff at about 21 keV. The X-ray absorption spectra were collected at room temperature in fluorescence mode, by a high-purity 13-element Ge detector. Using XAFS in grazing incidence [15] configuration, one can select the probed depth by varying the incidence angle of the incoming beam. X-ray absorption near-edge structure (XANES) spectra were simulated as a linear combination of the standard spectra for Cu^{+} and Cu^{2+} in soda lime glass [16], to obtain the information on the oxidation state of copper in different ion-exchanged regions. Extended X-ray absorption fine structure (EXAFS) region of the X-ray absorption coefficient was analyzed to have information about the local environment of copper ions, in term of interatomic distances, coordination numbers and Debye–Waller factors. To select the thickness of the probed region, measurements were taken for different beam incidence angles, ranging from 0.13 to 3.5 degrees

(with respect to the sample surface), corresponding to an attenuation length from about 4 nm to 5 μm, respectively. The attenuation lengths were calculated following the data tables [17]. As a standard reference, X-ray absorption spectra in transmission mode were recorded for Cu_2O and CuO crystalline powders, and for Cu bulk. EXAFS (extended X-ray absorption fine structure) data processing was carried out by Fourier filtering and multi-parameter fit in the R-space. Theoretical scattering amplitude and phase were generated by FEFF code [18] and the multi-electron amplitude reduction factor S_0^2 in standard EXAFS formula was fixed to the value obtained from standards spectra ($S_0^2 = 0.8 \pm 0.1$ for both CuO and Cu_2O). Copper and alkali ion concentration profiles were determined by secondary ion mass spectrometry using an IMS-4*f* CAMECA spectrometer, equipped with a normal incidence electron gun to compensate the surface charge build-up while profiling insulating samples. We used a 14.5 keV Cs^+ primary beam and negative secondary ion detection (rastered area: $125 \times 125\ \mu m^2$). The absolute values of concentrations were determined by Rutherford backscattering spectrometry (RBS) measurements.

3 Results

Concentration profiles from SIMS data are shown in Fig. 1 for a typical soda-lime doped sample, processed under the conditions described above. For a soda-lime matrix, the exchange takes place between copper and sodium (see Fig. 1). An accumulation of copper in the region near the surface is evident, giving rise to copper distribution profiles that cannot be described by the usual phenomenology for the diffusion of a single ion species. Previous studies evidenced that the resulting profiles are given by the contribution of both Cu^+ and Cu^{2+} species [11, 19, 20]. In particular, it has been suggested that Cu^{2+} diffuses directly from the bath in the very first exchanged region following an erfc profile, while the much more mobile Cu^+ species is distributed throughout the whole exchanged region, with a gaussian shape [11, 19, 20].

Previous XAFS studies [21–23] showed that copper ions in ion-exchanged soda-lime glass are mostly in the Cu^+ state, but this result does not distinguish the possible different location of the copper ion species within the doped layer, since data are integrated over the whole ion-exchanged layer. In order to quantitatively determine the relative amount of the two oxidation states for copper at different depths, and thus to test the validity of the assumption about the location of the two copper species, the Cu^+/Cu^{2+} ratio values were determined as a function of the depth from the collected X-ray absorption near-edge structure (XANES) data. In Fig. 2, the XANES spectra are reported, collected for different incidence angles, together with standard spectra for CuO and Cu_2O polycrystalline samples. In Fig. 2, the spectra obtained for incidence angles ranging from 0.13 deg to 3.5 deg, corresponding to attenuation lengths of 4 nm to 5 μm, respectively, are shown together with the simulations (dotted lines). The Cu^+/Cu^{2+} ratio varies from 30:70 at the surface up to 85:15 in the case of the spectrum collected at 3.5 deg of incidence (5 μm of attenuation length).

The local order was investigated, in terms of coordination number, interatomic distances and Debye–Waller factors, by EXAFS analysis. The moduli of the EXAFS Fourier transform (FT) with the relative fits are reported in Fig. 3 for Cu *K*-edge. Transformations were performed in the interval $k = 3$–$9.5\ Å^{-1}$ with a k^3-weight. The interatomic distances, coordination numbers and Debye–Waller factors, as obtained by the fitting procedure, are reported in Table 1, together with the data for reference standards.

The moduli of EXAFS FTs exhibit, for all the samples, only one peak that can be ascribed to copper coordination with oxygen atoms. No second shell correlation is suggested between alkali and copper ions, as already found in other investigation [15, 16, 21–23]. In the ion-exchanged samples, Cu atoms are expected to locate in the Na^+ sites, bound to non-bridging O atoms after the substitution in the glass matrix. Nevertheless, the Cu−O bond length, which varies from

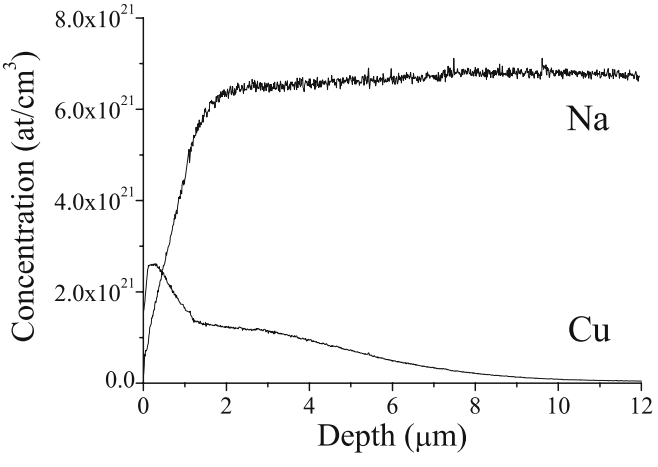

FIGURE 1 SIMS in-depth concentration profile of ion species taking part to ion exchange in soda lime glass. Exchange was performed in $CuSO_4$:Na_2SO_4 bath at 545 °C for 10 min

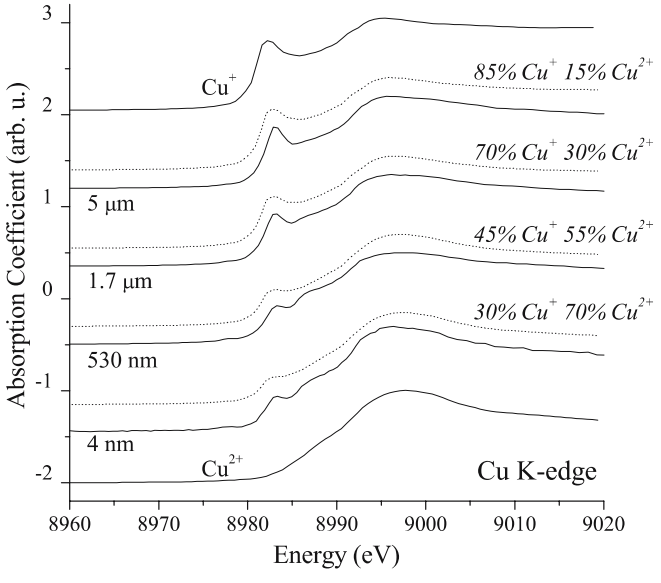

FIGURE 2 Cu *K*-edge absorption spectra collected for different incidence angles (*solid lines*), together with spectra of copper in glass with oxidation state (+1) and (+2), indicated as Cu^+ and Cu^{2+}. The simulated spectra are also reported (*dotted lines*). Respective attenuation lengths are also indicated

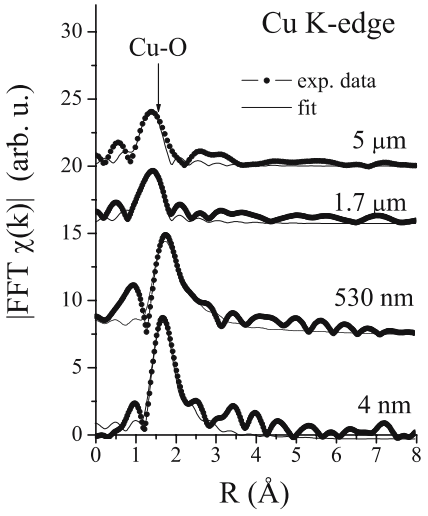

FIGURE 3 Moduli of Fourier transform for spectra (*dot*: experimental, *solid line*: fit) at Cu *K*-edge. Transformations were performed in the interval $k = 3$–9.5 Å^{-1} with a k^3-weight

	Cu−O coordination		
	R (Å)	N	$\sigma^2(10^{-4}$ Å$^2)$
4 nm	1.94 ± 0.03	3.8 ± 0.9	69 ± 42
530 nm	1.91 ± 0.03	2.9 ± 0.6	86 ± 44
1.7 μm	1.86 ± 0.03	2.8 ± 0.9	75 ± 44
5 μm	1.85 ± 0.03	2.8 ± 0.9	64 ± 43
CuO	1.95 ± 0.02	4	29 ± 12
Cu_2O	1.85 ± 0.02	2	16 ± 12

TABLE 1 Result of EXAFS analysis for the analyzed sample at Cu *K*-edge. R, N and σ^2 indicate, respectively, interatomic distance, coordination number and Debye–Waller factor. For the standards, N is fixed to the crystallographic values, while R and σ^2 derive from the fitting procedure

1.85 to 1.94 Å depending on the different incidence angles, is significantly shorter than the Na−O (2.30 Å) separation in glass, [24], and similar to the Cu−O bond length in copper oxides (1.85 Å in Cu_2O and 1.95 Å in CuO). This indicates that copper forms strong bonds with the matrix components and that structural rearrangements take place in the glass during the exchange process. The Cu−O bond length varies from 1.94 to 1.85 Å and the coordination numbers from 3.8 to 2.8 as the incidence angle increases (i.e., increasing the X-ray beam penetration depth), in agreement with XANES simulations that suggest an increase of Cu^+/Cu^{2+} ratio by increasing the probed depth. The EXAFS results for the spectra collected at 0.13 deg (i.e., 4 nm of penetration depth) are in agreement to values for the crystalline CuO oxide: copper coordinates 3.8 ± 0.9 oxygen atoms at a distance of (1.94 ± 0.03) Å. By increasing the penetration depth of the X-ray beam, the Cu−O average distance shifts to the typical value for Cu_2O oxide. The same trend is found for the coordination numbers. The values found for interatomic distances and coordination numbers are in agreement with previous investigations [22, 25, 26]. Indeed, the Debye–Waller factor values for the Cu−O bonds in the samples are larger than the ones for crystalline standards, due to the more disordered structure of the studied systems. Finally, it must be underlined that no metallic phases are present [15, 16, 21–23].

4 Discussion

The interdiffusion process between Cu^{2+}, Cu^+ and Na^+ was analyzed by means of the phenomenological model based on the Nernst–Planck expression [27, 28] for the ionic fluxes J:

$$J_{Cu^+} = -D_{Cu^+}\frac{\partial c_{Cu^+}}{\partial x} + \frac{eD_{Cu^+}}{kT}Ec_{Cu^+} \quad (1)$$

$$J_{Cu^{2+}} = -D_{Cu^{2+}}\frac{\partial c_{Cu^{2+}}}{\partial x} + \frac{2eD_{Cu^{2+}}}{kT}Ec_{Cu^{2+}} \quad (2)$$

$$J_{Na^+} = -D_{Na^+}\frac{\partial c_{Na^+}}{\partial x} + \frac{eD_{Na^+}}{kT}Ec_{Na^+} \quad (3)$$

where $c_i(x, t)$ are the ionic concentrations as a function of depth and time, D_i are the ionic self-diffusion coefficients, $z_i eD_i/kT$ are the ionic mobilities as from the Einstein relation, which are proportional to the ionic charge $z_i e$, and E is the local electric field. This term arises from the local charge unbalancing, which takes place due to the different mobility of the ionic species [28–30]. Under the hypothesis that the charge balance is locally maintained, the three equations are converted into two, thus giving the following conditions for the ionic fluxes and concentrations:

$$J_{Cu^+} + 2J_{Cu^{2+}} + J_{Na^+} = 0 \quad (4)$$

$$c_{Cu^+} + 2c_{Cu^{2+}} + c_{Na^+} = c_0 \quad (5)$$

where c_0 is the sodium bulk concentration in the glass. From (5), the following condition on the concentration gradients can be deduced:

$$\frac{\partial c_{Cu^+}}{\partial x} + 2\frac{\partial c_{Cu^{2+}}}{\partial x} + \frac{\partial c_{Na^+}}{\partial x} = 0. \quad (6)$$

The expression for the local electric field can be derived from (1)–(4):

$$E = \frac{kT/e}{D_{Cu^+}c_{Cu^+} + 4D_{Cu^{2+}}c_{Cu^{2+}} + D_{Na^+}c_{Na^+}} \times \left(D_{Cu^+}\frac{\partial c_{Cu^+}}{\partial x} + 2D_{Cu^{2+}}\frac{\partial c_{Cu^{2+}}}{\partial x} + D_{Na^+}\frac{\partial c_{Na^+}}{\partial x}\right). \quad (7)$$

By substituting this expression in (1) and (2), the flux equations for the two copper ionic species take the form:

$$J_{Cu^+} = -D_{11}\frac{\partial c_{Cu^+}}{\partial x} - D_{12}\frac{\partial c_{Cu^{2+}}}{\partial x} \quad (8)$$

$$J_{Cu^{2+}} = -D_{21}\frac{\partial c_{Cu^+}}{\partial x} - D_{22}\frac{\partial c_{Cu^{2+}}}{\partial x} \quad (9)$$

where

$$D_{11} = \frac{D_{Cu^+}(4D_{Cu^{2+}} - 2D_{Na^+})c_{Cu^{2+}} + D_{Cu^+}D_{Na^+}c_0}{(D_{Cu^+} - D_{Na^+})c_{Cu^+} + (4D_{Cu^{2+}} - 2D_{Na^+})c_{Cu^{2+}} + D_{Na^+}c_0} \quad (10)$$

$$D_{12} = \frac{2D_{Cu^+}(D_{Cu^{2+}} - D_{Na^+})c_{Cu^+}}{(D_{Cu^+} - D_{Na^+})c_{Cu^+} + (4D_{Cu^{2+}} - 2D_{Na^+})c_{Cu^{2+}} + D_{Na^+}c_0} \quad (11)$$

$$D_{22} = \frac{D_{Cu^{2+}}(D_{Cu^+} - D_{Na^+})c_{Cu^+} + 2D_{Cu^{2+}}D_{Na^+}c_{Cu^{2+}} + D_{Cu^{2+}}D_{Na^+}c_0}{(D_{Cu^+} - D_{Na^+})c_{Cu^+} + (4D_{Cu^{2+}} - 2D_{Na^+})c_{Cu^{2+}} + D_{Na^+}c_0} \quad (12)$$

$$D_{21} = \frac{2D_{Cu^{2+}}(D_{Cu^+} - D_{Na^+})c_{Cu^{2+}}}{(D_{Cu^+} - D_{Na^+})c_{Cu^+} + (4D_{Cu^{2+}} - 2D_{Na^+})c_{Cu^{2+}} + D_{Na^+}c_0}. \quad (13)$$

If the surface concentration of Cu^+ and Cu^{2+} are assumed to be constant during the process (the molten bath acts as an infinite supplier), the evolution of the concentration profiles can be determined by integrating the equations:

$$\frac{\partial c_{Cu^{2+}}}{\partial t} = -\frac{\partial J_{Cu^{2+}}}{\partial x} \quad (14)$$

$$\frac{\partial c_{Cu^+}}{\partial t} = -\frac{\partial J_{Cu^+}}{\partial x} \quad (15)$$

where the ionic fluxes are given by (8) and (9) and with the boundary conditions (for the normalized concentrations, atomic fraction):

$$c_{Cu^{2+}}(t, x = 0) = c^0_{Cu^{2+}} = \text{const.} \quad (16)$$

$$c_{Cu^+}(t, x = 0) = c^0_{Cu^+} = \text{const.} \quad (17)$$

Equations (14) and (15) were integrated by means of a standard explicit finite difference method, where the surface concentration values are assumed to be constant to the values $c^0_{Cu^{2+}} = 0.33$, $c^0_{Cu^+} = 0.17$. These values, which are normalized to the bulk sodium concentration in the glass, are calculated from the experimental surface concentration and from the Cu^+/Cu^{2+} measured surface ratio.

To study the role of the different parameters in the migration mechanism, the concentration profiles of the two copper ionic species were calculated for a 10 minutes interdiffusion process by taking different values for the self-diffusion coefficients. The order of magnitude of the copper diffusion coefficients can be obtained from the observed penetration depth values, since no data are available in the literature for most of copper diffusion parameters in glass. On the other hand, the sodium self-diffusion coefficient is reported for soda-lime glass networks of similar composition [31]. The self-diffusion coefficients for Cu^{2+}, Cu^+ and Na^+ are, therefore, evaluated of about 10^{-12}, 10^{-10} and 10^{-9} cm^2/s, respectively. The most interesting result is that the correlation effects between the ionic fluxes give rise to a Cu^+ diffusion profile with a maximum below the surface (see Fig. 4a), while the Cu^{2+} concentration profile is quite similar to that observed for an interdiffusion process of only two ionic species. This finding is in contrast with the reported hypothesis that copper diffusion as measured by SIMS is simply due to a superposition of an erfc with a gaussian profile. Basically, the different behavior of the two ionic species must be ascribed to their different mobilities, which are directly related to the respective diffusion structure (pointed out by EXAFS results) strongly affect the jump from one site to another in the glass network, giving rise to quite different diffusion behaviors. To evidence the role in the migration process of the different self-diffusion coefficients, they were varied by one order of magnitude, from 8×10^{-13} to 5×10^{-12} cm^2/s for Cu^{2+}, from 5×10^{-11} to 2×10^{-10} cm^2/s for Cu^+ and from 10^{-9} to 10^{-8} cm^2/s for Na^+. From this analysis, it was found that the Cu^+ profile is strongly affected by the self-diffusion parameter values of both the copper ion species, while the Cu^{2+} profile does not change appreciably by varying the Cu^+ self-diffusion coefficient. On the other hand, the variation of the Na^+ self-diffusion coefficient did not give a significant modification of the copper species profiles. These findings are consistent with the results obtained in the case of the interdiffusion of two species only, where the final concentration profiles are determined mainly by the transport parameters of the slower ion. In Fig. 4 are reported the partial (a) and total (b) copper concentration profiles, respectively, as calculated after 10 minutes of interdiffusion time and by using for self-diffusion coefficients the values: $D_{Cu^{2+}} = 2 \times 10^{-12}$ cm^2/s, $D_{Cu^+} = 1 \times 10^{-10}$ cm^2/s and $D_{Na^+} = 6 \times 10^{-9}$ cm^2/s.

At this stage of the model, the interesting result is the accumulation of Cu^+ below the surface, with a distribution profile exhibiting a maximum towards 2 μm depth. Indeed, this feature should be expected to explain XANES results, as discussed above.

The very poor agreement between the experimental and the calculated curves for total Cu (Fig. 4b) is due to two simplifying assumptions which the model is based on. First, the diffusion coefficient and the ionic mobility are supposed to follow the Einstein relation. Second, the diffusion coefficients are taken as constant during the entire interdiffusion process. Indeed, it is clear also from literature [3, 22, 25, 26] that during the ion-exchange process the glass network under-

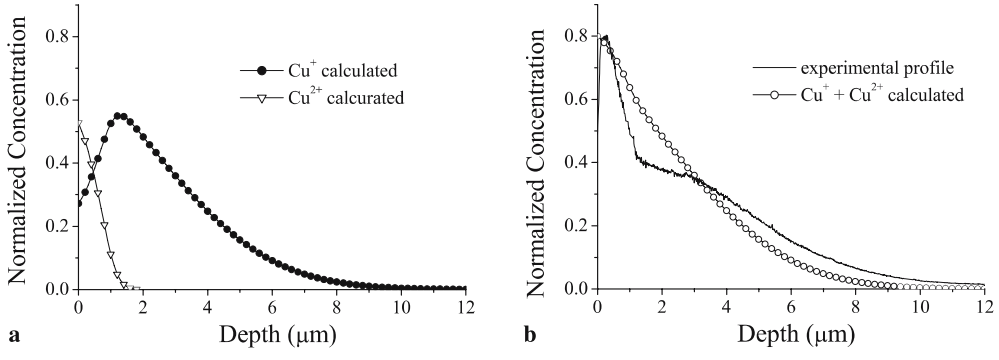

FIGURE 4 Partial **a** and total **b** copper diffusion profiles calculated after 10 minutes of interdiffusion total time and by using the following values for the self-diffusion coefficient: $D_{Cu^{2+}} = 2 \times 10^{-12}$ cm^2/s, $D_{Cu^+} = 1 \times 10^{-10}$ cm^2/s and $D_{Na^+} = 6 \times 10^{-9}$ cm^2/s

goes concentration-dependent structural changes, owing to local coordination rearrangements at the ion sites. Therefore, to give a complete description of the interdiffusion process in ion-exchanged glasses, it is necessary to assume that the diffusion coefficient of the individual ions depends on the concentration due to the modification of the local structure. This kind of problem has been extensively studied in the case of mixed-alkali glasses, where the transport parameters of ion species nonlinearly depend on the concentration [32]. This behavior is mainly attributed to the effect of the composition on the activation energy of the self-diffusion coefficient D, which follows an Arrhenius-type relationship:

$$D = D_0 \exp\left(-\frac{\Delta E}{kT}\right) \tag{18}$$

where ΔE is the activation energy for the ion diffusion between two adjacent sites. In particular, it has been established that the activation energy barrier for alkali ion diffusion in glasses is affected mostly by the interaction energy with the different types of surrounding ions [32–34].

The potential energy for the ion located into a glass site depends on the interaction energies with neighbors, i.e., an alkali ion having a stronger bond with neighbors is in a deeper potential well, giving rise to a decrease of the diffusion coefficient. During diffusion, the concentrations of the different ionic species affect the potential energy owing to the change of both the neighbors atoms and the interatomic distances due to the modification of the local network structure. For ion-exchanged glasses, an approach similar to mixed-alkali systems can, thus, be used [35]. In the case of the copper diffusion process, we integrated the interdiffusion equations by supposing diffusion coefficients following the Arrhenius relationship with concentration dependent activation energies. In particular, the activation energy of each ion is to depend on the concentrations of the three ion species involved in the interdiffusion process. For instance, the activation energy $\Delta E\,(\mathrm{Cu}^+)$ of Cu^+ has the following expression:

$$\begin{aligned}\Delta E\,(\mathrm{Cu}^+) = \Delta E^0\,(\mathrm{Cu}^+) &+ X(\mathrm{Cu}^+)\Delta E\,(\mathrm{Cu}^+ - \mathrm{Cu}^+) \\ &+ X(\mathrm{Cu}^{2+})\Delta E\,(\mathrm{Cu}^+ - \mathrm{Cu}^{2+}) \\ &+ X(\mathrm{Na}^+)\Delta E\,(\mathrm{Cu}^+ - \mathrm{Na}^+)\end{aligned} \tag{19}$$

where $\Delta E^0\,(\mathrm{Cu}^+)$ is the activation energy excluding the contribution of the neighboring ions, $X(i)$ are the ionic fractions of the different species, and $\Delta E\,(\mathrm{Cu}^+ - i)$ are the interaction energies between Cu^+ and the neighboring ions involved in the interdiffusion process. Following this approach, the interdiffusion equation were integrated by supposing concentration-dependent activation energies as from (19), where the first term is included in the pre-exponential factor D_0. The pre-exponential factors and the activation energies were varied such to reproduce both the copper diffusion profile obtained from SIMS measurements and the $\mathrm{Cu}^+/\mathrm{Cu}^{2+}$ integrated ratio as a function of the depth obtained from XANES measurements. In Fig. 5, experimental data and theoretical curves are shown, obtained with the parameters reported in Table 2. The good agreement between the $\mathrm{Cu}^+/\mathrm{Cu}^{2+}$ ratio as a function of the depth and the experimental XANES $\mathrm{Cu}^+/\mathrm{Cu}^{2+}$ ratio is shown in Fig. 6. Each point represents the ratio integrated from the surface up to the corresponding depth.

The obtained energy values are comparable with those reported in the literature, where the mixed-alkali effect for sodium and potassium is studied following this model [32–34], and where values ranging from 0.5 to 1.5 eV are indicated for the activation energies of potassium in binary silicate glasses. As concerns the pre-exponential factors, their choice is certainly less critical for the fit procedure with respect to the activation energies. In any case, the parameter for Na^+ is in agreement with literature data [31], and the copper ones are correspondingly reliable.

It must be underlined that the interdiffusion model we used to describe copper-sodium ion-exchange does not include any red-ox kinetics of copper ions during the process. This phenomenon is still a matter of debate in the case of copper-containing glasses produced from melts. In particular, it was established that the equilibrium $\mathrm{Cu}^+/\mathrm{Cu}^{2+}$ ratio in these systems depends on a large number of parameters, notably the

parameters	values
$D^0_{\mathrm{Cu}^+}$	3.5×10^{-13} cm^2/s
$D^0_{\mathrm{Cu}^{2+}}$	9.5×10^{-19} cm^2/s
$D^0_{\mathrm{Na}^+}$	9.5×10^{-11} cm^2/s
$\Delta E\,(\mathrm{Cu}^+ - \mathrm{Cu}^+)$	0.6 eV
$\Delta E\,(\mathrm{Cu}^+ - \mathrm{Cu}^{2+})$	0.05 eV
$\Delta E\,(\mathrm{Cu}^+ - \mathrm{Na}^+)$	0.4 eV
$\Delta E\,(\mathrm{Cu}^{2+} - \mathrm{Cu}^{2+})$	1.1 eV
$\Delta E\,(\mathrm{Cu}^{2+} - \mathrm{Na}^+)$	1.2 eV
$\Delta E\,(\mathrm{Na}^+ - \mathrm{Na}^+)$	0.4 eV

TABLE 2 Values of pre-exponential factors and interaction energies used for the interpolation of the experimental data reported in Fig. 5

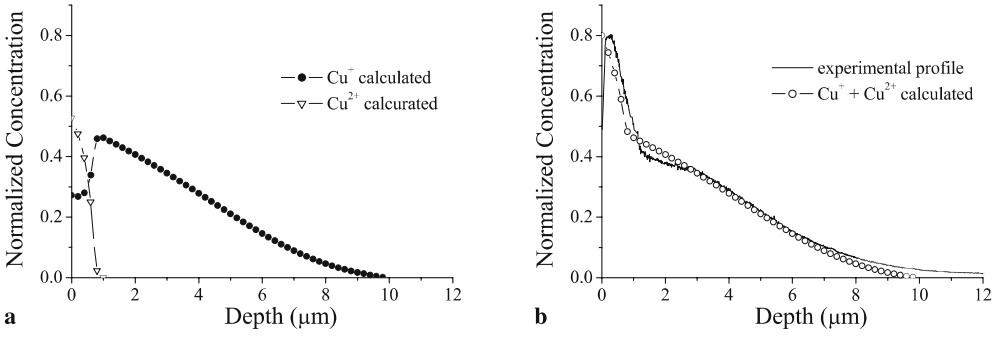

FIGURE 5 Partial **a** and total **b** copper diffusion profiles calculated after 10 minutes of interdiffusion total time and by using values reported in Table 2

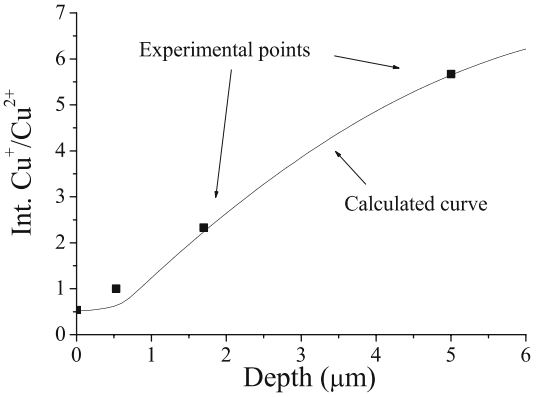

FIGURE 6 Cu^{+}/Cu^{2+} ratio as a function of the depth for the profiles of Fig. 5 compared with XANES Cu^{+}/Cu^{2+} ratio

melting procedures, the sample thermal history and the glass composition [35]. Moreover, the equilibrium conditions can be reached only after several hours of heating. As far as the surface processes are concerned, it can be assumed that the salt bath at the beginning of the process contains only Cu^{2+} ions. Therefore, the main chemical modification in the salt phase, and notably at the glass surface, can be only a reduction process from Cu^{2+} to Cu^{+}. Since this kind of transformation has been observed by Sakka [12] for chloride salts, it can be assumed to occur also for sulphate salts. We, therefore, integrated the interdiffusion equation systems taking into account that stationary value of the species surface concentration is reached within few minutes, as indicated by XANES results. After this time, the shape of the diffusion profiles becomes indistinguishable from that obtained starting from constant surface concentration values. This result suggests that the bulk migration mechanisms are those which determine the shape of the concentration profiles, once the surface phenomena have reached the equilibrium. In bulk glass, if any kinetic red-ox process occurs, it is much slower than that which drives the reduction mechanism at the surface [36, 37].

Taking into account these results, we can conclude that the copper migration mechanism can be completely described by supposing that the surface ionic concentrations are constant since the first exchange steps, and no red-ox mechanisms is present into the glass matrix. This result does not definitely discard the presence of some red-ox process at the surface or into the bulk of the glass, but these effects are certainly not important for the copper migration.

5 Conclusion

X-ray absorption near-edge structure spectroscopy in grazing incidence mode and secondary ion mass spectrometry were performed on Cu-doped ion-exchanged soda-lime glasses. A model was developed for the description of the diffusion process. The main conclusions that can be drawn are:

- The interdiffusion process between Cu^{+}, Cu^{2+} and Na^{+} is governed by correlation effects between the ionic fluxes, giving rise to a copper distribution which is strongly dependent on the transport parameters of all the species involved in the process.
- The Cu^{+} diffusion profile exhibits a maximum below the surface. This behavior is peculiar of an ion exchange process involving more than two species, which is described here for the first time. On the other hand, Cu^{2+} diffusion follows a monotonic decreasing distribution.
- The diffusion coefficients and so the activation energies came out to depend on the local ionic concentration. This is related to the local structure modification, evidenced also by XAFS measurements.
- The ion exchange process has been described by a model that for the first time points out the relation between the observed phenomena and the mixed-alkali effect.
- The migration of the two copper ions is governed by the dynamics of the diffusion, while the chemistry of copper states equilibrium plays a negligible role.
- Synchrotron radiation-based techniques are crucial in the determination of the structure of ion-exchanged glasses. In particular, the use of grazing incidence configuration allowed to discriminate the different ionic states as a function of the depth, giving also information on the local order around each species.

REFERENCES

1 R.V. Ramaswamy, R. Srivastava: IEEE J. Lightwave Technol. **6**, 984 (1988) and references therein
2 R. Debnath: J. Lumin. **43**, 375 (1989)
3 E. Borsella, A. Dal Vecchio, M.A. Garcia, C. Sada, F. Gonella, R. Polloni, A. Quaranta, L.J.G.W. Van Wilderen: J. Appl. Phys. **91**, 1 (2002)
4 F. Gonella, P. Mazzoldi: *Handbook of Nanostructured Materials and Nanotechnology*, Vol. 4 (Academic Press, S. Diego, h.s. nalwa edition 2000)
5 U. Kreibig, M. Vollmer: Optical Properties of Metal Clusters, Vol. 25 of Springer Series in Materials Science (Springer, Berlin 1995)
6 E. Cattaruzza, G. Battaglin, F. Gonella, R. Polloni, C. Mattei, G. Maurizio, P. Mazzoldi, C. Sada, M. Montagna, C. Tosello, M. Ferrari: Philos. Mag. B, **82**, 735 (2002)
7 P. Mazzoldi, G.W. Arnold, G. Battaglin, F. Gonella, R.F. Haglund Jr.: J. Nonlin. Opt. Phys. Mater. **5**, 285 (1996)
8 S. Gevorgyan: Electron. Eng. (U.K.) **26**, 38 (1990)
9 T. Yoko, T. Nishiwaki, K. Kamiya, S. Sakka: J. Am. Ceram. Soc. **74**, 1104 (1991)
10 H. Marquez, D. Salazar, A. Villalobos, G. Paez, J.Ma. Rincon: Appl. Opt. **34**, 5817 (1995)
11 F. Gonella, F. Caccavale, L.D. Bogomolova, F. D'Acapito, A. Quaranta: J. Appl. Phys. **83**, 1200 (1998)
12 S. Sakka, K. Kamiya, K. Kato: J. Non-Cryst. Solids **52**, 77 (1982)
13 I. Davoli, H.N. Thanh, F. D'Acapito: AIP Conference Proceedings, Vol. 652 (2003) p. 388
14 S. Pascarelli, F. Boscherini, F. D'Acapito, J. Hrdy, C. Meneghini, S. Mobilio: J. Synchr. Rad. **3**, 147 (1996)
15 F. D'Acapito, I. Davoli, P. Ghigna, S. Mobilio: J. Synchr. Rad. **10**, 260 (2003)
16 F. D'Acapito, S. Mobilio, J. Regnard, E. Cattaruzza, F. Gonella, P. Mazzoldi: J. Non-Cryst. Solids **232**–**234**, 364 (1998)
17 B.L. Henke, E.M. Gullison, J.C. Davis: X-ray interaction: photoabsorption, scattering, transmission, and reflection at $E = 50$–$30\,000$ eV, $Z = 1 - 92$, Vol. 54 of Atomic Data and Nuclear Data Tables (1993)
18 A.L. Ankudinov, B. Ravel, J.J. Rehr, S.D. Conradson: Phys. Rev. B **58**, 7565 (1998)
19 F. Gonella: Appl. Phys. Lett. **69**, 314 (1996)
20 F. Gonella, F. Caccavale, A. Quaranta, A. Sambo: J. Mod. Opt. **45**, 837 (1998)
21 F. D'Acapito, S. Colonna, S. Mobilio, F. Gonella, E. Cattaruzza, P. Mazzoldi: Appl. Phys. Lett. **71**, 261 (1997)
22 J. Lee, T. Yano, S. Shibata, A. Nukui, M. Yamane: J. Non-Cryst. Solids **277**, 155 (2000)
23 C. Maurizio, F. D'Acapito, M. Benfatto, S. Mobilio, E. Cattaruzza, F. Gonella: Eur. Phys. J. B **14**, 211 (2000)

24 G.N. Greaves, A. Fontaine, P. Lagarde, D. Raoux, S.J. Gurman: Nature **293**, 611 (1981)
25 G.N. Greaves, S.J. Gurman, C.R. Catlows, A.V. Chadwick, S.N. Houde-Walter, C.M.B. Henderson, B.R. Dobson: Philos. Mag. A **64**, 1059 (1991)
26 F. D'Acapito, F. Gonella, E. Cattaruzza, S. Pascarelli, P. Mazzoldi, S. Mobilio: Nucl. Instrum. Methods Phys. Res., Sect. B **120**, 110 (1996)
27 G. Schulze: Angew. Phys. **40**, 335 (1913)
28 R.H. Doremus: *Modern Aspects of the Vitreous State*, Vol. 4 (butterworth and co. ltd. edition, London 1962)
29 A. Quaranta, F. Gonella: J. Non-Cryst. Solids **192**–**193**, 334 (1995)
30 R.H. Doremus: J. Phys. Chem. **68**, 2212 (1964)
31 N.P. Bansal, R.H. Doremus: *Handbook of glass properties* (Academic Press, London 1986)
32 M. Tomozawa: J. Non-Cryst. Solids **152**, 59 (1993)
33 G. N. Greaves, K. L. Ngai: J. Non-Cryst. Solids **172**, 1378 (1994)
34 G. N. Greaves, K. L. Nagai: Phys. Rev. B **52**, 6358 (1995)
35 P. Mazzoldi, A. Miotello: J. Non-Cryst. Solids **94**, 897 (1987)
36 J.L. Barton, M. De Billy: J. Nonlin. Opt. Phys. Mater. **38**–**39**, 523 (1980)
37 J.A. Duffy: J. Non-Cryst. Solids **196**, 45 (1996)